SYMCOMP 2015
Faro, March 26-27, 2015

6TH-ORDER FINITE VOLUME APPROXIMATIONS FOR THE STOKES EQUATIONS WITH A CURVED BOUNDARY

Ricardo Costa[1*], Stéphane Clain[1,2] Gaspar J. Machado[1]

1: Centre of Mathematics
School of Science
University of Minho
Campus de Azurm, 4800-058 Guimares, Portugal
e-mail: pg24046@alunos.uminho.pt,{clain,gjm}@math.uminho.pt

2: Institut de Mathématiques de Toulouse
Université Paul Sabatier
31062 Toulouse, France

Keywords: finite volume, sixth-order approximation, Stokes equation, curved boundary

Abstract. *A new solver for the Stokes equations based on the finite volume method is proposed using very accurate polynomial reconstruction to provide a 6th-order scheme. We face two main difficulties: the gradient-divergence duality where the divergence free condition will impose the pressure gradient, and on the other hand, we assume that the domain has a regular curved boundary. The last point implies that a simple approximation of the boundary using piecewise segment lines dramatically reduces the scheme accuracy to at most a second-order one. We propose a new and simple technology which enables to restore the full scheme accuracy based on a specific polynomial reconstruction only using the Gauss points of the curved boundary and does not require any geometrical transformation.*

1 INTRODUCTION

The Stokes or Navier-Stokes equations represent critical issues in modelling and simulations since they encompass within a lot of applications and accurate numerical simulations turns to be a big challenge to provide approximations. Since the finite element method is still the major technique to tackle the discretisation question, finite volume method has received considerable attention due to its intrinsics qualities: built-in conservative and versatility. We refer to the pioneer book of Patankar [16] and the textbook of Ferziger and Peric [7] for an overview of the finite volume for the Navier-Stokes equations.
Very high-order schemes for incompressible fluid flow have been developed using the finite difference framework with the Padé methodology (the so-called compact scheme) [11] on staggered structured grids (see [12][9] and references herein) providing fourth-order or sixth-order approximations [3]. Finite element [10][8] and discontinuous Galerkin methods [13][6][14] also received important contributions to achieve very high-order approximation both in time and space. Sixth-order finite volume approximation is the current state-of-the-art on structured using compact schemes but the unstructured mesh case is still confidential and remains a important issue.
When dealing with very-high order scheme, a crucial point is the evaluation of boundary conditions when the domain is curved. Finite elements or Discontinuous Garlekin methods used isoparametric elements which turns the implementation very complex while the finite volume approach is simpler. Two techniques have been proposed in the convection diffusion context. The first one directly used the Gauss points on the curved boundary to achieve polynomial reconstructions [15] whereas the second one used the Gauss points on the segment for the polynomial reconstruction but adjust a free parameter to reproduce the Dirichlet condition at the Gauss points of the curve [4].
We present a finite volume scheme to provide a sixth-order approximation of the solution of the Stokes problem involving curved boundary. We use a staggered discretization with a primal unstructured mesh for the pressure and the associated diamond mesh for the velocity to avoid the Rhie-Chow interpolation [17][20]. The coupled velocity-pressure approach is employed to avoid the pressure correction intermediate step to provide the divergence-free velocity [9]. Moreover, we do not treat the steady-state as the asymptotic limit of an artificial time marching problem but we directly solve the linear system associated to the saddle point problem. The main difficulty is to achieve an efficient approximation of the solution taking into account the divergence-free velocity constraint to determine the pressure. The method is based, on the one hand, in different kinds of polynomial reconstructions to compute the viscous flux, the pressure gradient, the velocity divergence up to a sixth-order of accuracy and, on the other hand, in a matrix-free formulation using the residual method as in [5][4] solve with the algebraic solver GMRES [19][18]. We detail in the paper the specific treatment of Dirichlet conditions with curved boundary. Indeed, a straightforward approximation using the polygonal domain will lead to a strong degradation of the order (at most second-order) and correction of the

traditional reconstruction will be implemented to recover the optimal order. We design a new local reconstruction involving a free parameter to be fixed such that the Dirichlet conditions on the curved boundary are satisfied. Numerical tests are carried out to prove the efficiency of the method.
The paper is organized as follow. Section 2 presents the generic finite volume scheme for very high order approximation in the context of the Stokes equations. In the third section we tackle the question of the polynomial reconstructions while section four is dedicated to the specific case of the curved boundary. In section 5, we present the numerical results and end the paper with a short conclusion.

2 FINITE VOLUME SCHEME FOR THE STOKES EQUATIONS

Let Ω be an open bounded domain of $\mathbb{R}^2$ with boundary $\partial\Omega$ and $x = (x_1, x_2)$. We seek functions $U = (U_1, U_2) \equiv (U_1(x), U_2(x))$, the velocity field, and $P \equiv P(x)$, the pressure, solutions of the steady-state flow of an incompressible Newtonian fluid governed by the Stokes equations

$$\nabla \cdot (-\mu \nabla U + P I_2) = f, \qquad \text{in } \Omega, \tag{1}$$

$$\nabla \cdot U = 0, \qquad \text{in } \Omega, \tag{2}$$

where the dynamic viscosity $\mu \equiv \mu(x)$ and the source term $f = (f_1, f_2) \equiv (f_1(x), f_2(x))$ are given regular functions. The tensor ∇U is defined as $[\nabla U]_{\alpha\beta} = \frac{\partial U_\alpha}{\partial x_\beta}$, $\alpha, \beta = 1, 2$, and I_2 stands for the identity matrix in $\mathbb{R}^{2\times 2}$. The system (1-2) is completed with the Dirichlet boundary condition

$$U = U_{\mathrm{D}}, \qquad \text{on } \partial\Omega, \tag{3}$$

where $U_{\mathrm{D}} = (U_{1,\mathrm{D}}, U_{2,\mathrm{D}}) \equiv (U_{1,\mathrm{D}}(x), U_{2,\mathrm{D}}(x))$ is a given regular function on $\partial\Omega$ which satisfies the compatibility condition

$$\int_{\partial\Omega} U_{\mathrm{D}} \cdot n \, \mathrm{d}s = 0,$$

with $n = (n_1, n_2)$ the outward unit normal vector on $\partial\Omega$. Moreover, uniqueness for the pressure is guaranteed by the additional constraint $\int_\Omega P \, \mathrm{d}x = 0$.

2.1 Primal and diamond meshes

The primal mesh of Ω, that we denote by $\mathcal{M}$, is a partition of Ω into I non-overlapping convex polygonal cells c_i, $i \in \mathcal{C}_\mathcal{M} = \{1, \ldots, I\}$, and adopt the notations we detail hereafter (see Fig. 1, left):

- for any cell c_i, $i \in \mathcal{C}_\mathcal{M}$, we denote by ∂c_i its boundary and by $|c_i|$ its area; the reference cell point is denoted by m_i which can be any point in c_i (in the present work we shall consider the centroid);

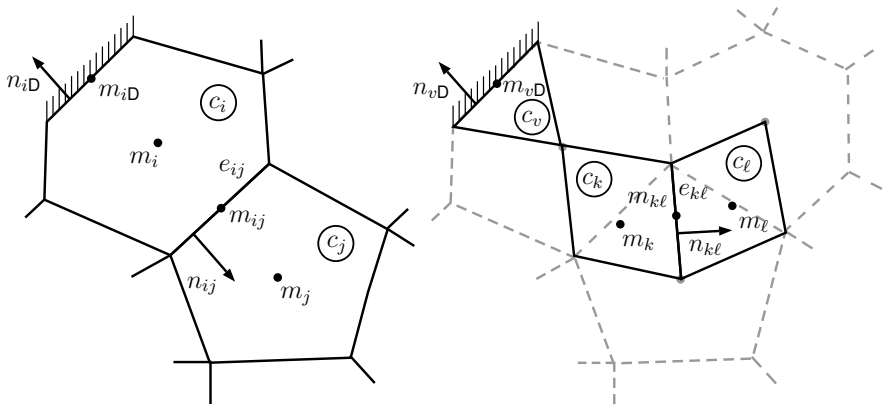

Figure 1: Notation for the primal mesh (left) and for the diamond mesh (right).

- two cells c_i and c_j share a common edge e_{ij} whose length is denoted by $|e_{ij}|$ and $n_{ij} = (n_{1,ij}, n_{2,ij})$ is the unit normal vector to e_{ij} outward to c_i, *i.e.* $n_{ij} = -n_{ji}$; the reference edge point is m_{ij} which can be any point in e_{ij} (in the present work we consider the midpoint); if an edge of c_i belongs to the boundary, the index j is tagged by the letter D;

- for any cell c_i, $i \in \mathcal{C}_\mathcal{M}$, we associate the index set $\nu(i) \subset \{1, \cdots, I\} \cup \{\mathrm{D}\}$ such that $j \in \nu(i)$ if e_{ij} is a common edge of cells c_i and c_j or with the boundary if $j = \mathrm{D}$.

The diamond mesh of Ω, that we denote by $\mathcal{D}$, derives from the primal mesh $\mathcal{M}$ and is constituted of K non-overlapping diamond-shape cell (which degenerate to triangles in the boundary) c_k, $k \in \mathcal{C}_\mathcal{D} = \{I+1, \ldots, I+K\}$. Indeed, for each inner primal edge e_{ij} corresponds a unique cell of the diamond mesh defined by the reference points m_i and m_j and the vertices of the edge (the dual cell associated to a boundary edge $e_{i\mathrm{D}}$ is defined by the reference point m_i and the vertices of the edge).
The notation for the diamond mesh follows the notation introduced for the primal mesh where we substitute the index $i \in \mathcal{C}_\mathcal{M}$ by $k \in \mathcal{C}_\mathcal{D}$ and the index $j \in \nu(i)$ by $\ell \in \nu(k)$ (see Fig. 1, right). In particular m_k is any point in c_k (in the present work we shall consider the centroid) and $m_{k\ell}$ is any point in $e_{k\ell}$ (in the present work we consider the midpoint).
To define the association between diamond cells and primal edges, we introduce the correspondence operator $\Pi_\mathcal{D}$ such that for given arguments (i,j), $i \in \mathcal{C}_\mathcal{M}$, $j \in \nu(i)$, we associate the corresponding diamond cell index $k = \Pi_\mathcal{D}(i,j) \in \mathcal{C}_\mathcal{D}$. In the same way, for each diamond edge, we introduce the correspondence operator $\Pi_\mathcal{M}$ such that for given arguments (k,ℓ), $k \in \mathcal{C}_\mathcal{D}$, $\ell \in \nu(k)$, we associate the corresponding primal cell index $i = \Pi_\mathcal{M}(k,\ell) \in \mathcal{C}_\mathcal{M}$.
The numerical integrations on the edges are performed with Gaussian quadrature where for the primal edges e_{ij}, $i \in \mathcal{C}_\mathcal{M}$, $j \in \nu(i)$, we denote by $q_{ij,r}$, $r = 1, \ldots, R$, their Gauss points and for the diamond edges $e_{k\ell}$, $k \in \mathcal{C}_\mathcal{D}$, $\ell \in \nu(k)$, we denote by $q_{k\ell,r}$, $r = 1, \ldots, R$,

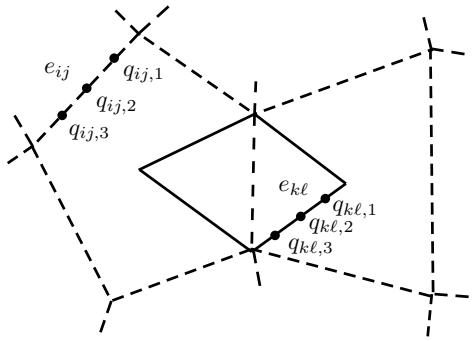

Figure 2: Gauss points on the edges of the primal cells (dashes lines) and on the edges of the diamond cells (solid lines).

their Gauss points, both sets with weights ζ_r, $r = 1, \ldots, R$ (see Fig. 2).

2.2 Generic finite volume scheme

To provide the generic very high-order finite volume scheme, we first integrate equation (1) over each diamond cell c_k, $k \in \mathcal{C}_\mathcal{D}$, and then apply the divergence theorem, yielding

$$\int_{\partial c_k} (-\mu \nabla U + P I_2)\, n \, \mathrm{d}s = \int_{c_k} f \, \mathrm{d}x,$$

which can be rewritten in the scalar form as

$$\int_{\partial c_k} (-\mu \nabla U_\beta \cdot n + P n_\beta) \, \mathrm{d}s = \int_{c_k} f_\beta \, \mathrm{d}x, \ \beta = 1, 2.$$

Considering the Gaussian quadrature with R points, *i.e.* of order $2R$, for the line integrals, we get the residual expression

$$\sum_{\ell \in \nu(k)} \frac{|e_{k\ell}|}{|c_k|} \left[\sum_{r=1}^{R} \zeta_r \left(\mathbb{F}^U_{\beta,k\ell,r} + \mathbb{F}^P_{\beta,k\ell,r} \right) \right] - f_{\beta,k} = \mathcal{O}\left(h_k^{2R} \right), \ \beta = 1, 2, \tag{4}$$

with the physical fluxes given by

$$\mathbb{F}^U_{\beta,k\ell,r} = -\mu(q_{k\ell,r}) \nabla U_\beta(q_{k\ell,r}) \cdot n_{k\ell}, \quad \mathbb{F}^P_{\beta,k\ell,r} = P(q_{k\ell,r}) n_{\beta,k\ell},$$

$h_k = \max_{\ell \in \nu(k)} |e_{k\ell}|$, and $f_{\beta,k}$ an approximation of order $2R$ of the mean value of f_β over cell c_k (if cell c_k is not triangular, we split it into sub-triangles which share the cell centroid as a common vertex and apply the quadrature rule on each sub-triangle as in [**?**]).
We now integrate equation (2) over each primal cell c_i and apply again the divergence theorem, yielding

$$\int_{\partial c_i} U \cdot n \, \mathrm{d}s = 0.$$

Considering again Gaussian quadrature with R points for the line integrals, we get the residual expression

$$\sum_{j\in\nu(i)} \frac{|e_{ij}|}{|c_i|} \sum_{r=1}^{R} \zeta_r \, \mathbb{F}^{\nabla}_{ij,r} = O(h_i^{2R}), \tag{5}$$

with the physical flux given by

$$\mathbb{F}^{\nabla}_{ij,r} = U(q_{ij,r}) \cdot n_{ij}$$

and $h_i = \max_{j\in\nu(i)} |e_{ij}|$.

3 POLYNOMIAL RECONSTRUCTIONS

The polynomial reconstruction is a powerful tool to provide an accurate local representation of the underlying solution and was initially introduced in [1, 2] for hyperbolic problems. In [5] a new methodology was proposed in the context of convection-diffusion problems in order to achieve very accurate approximations of the gradient fluxes and to take into account the boundary conditions. The authors introduced different types of polynomial reconstructions namely the conservative reconstruction in cells and on Dirichlet boundary edges and the non-conservative reconstruction on inner edges, in order to compute approximations of the convective and the diffusive fluxes. We now adapt this technology for the specific Stokes problem where the main difficulty is to handle the two meshes.

3.1 Stencil and data

A stencil is a collection of cells situated in the vicinity of a reference geometrical entity, namely an edge or a cell where the number of elements of the stencil shall depend on the degree d of the polynomial function we intend to construct. For each diamond edge $e_{k\ell}$, $k \in \mathcal{C}_{\mathcal{D}}$, $\ell \in \nu(k)$, we associate the stencil $S_{k\ell}$ consisting of the indices of neighbor diamond cells. Analogously, we associate the stencil S_k for each diamond cell c_k, $k \in \mathcal{C}_{\mathcal{D}}$, and the stencil S_i for each primal cell c_i, $i \in \mathcal{C}_{\mathcal{M}}$, consisting of the indices of neighbor dual and primal cells, respectively. Remark. *A polynomial reconstruction of degree d requires $n_d = (d+1)(d+2)/2$ coefficients. So, in practice, a stencil consists of the N_d closest cells to each geometrical entity (edge or cell) in the respective mesh, with $N_d \geq n_d$ (we consider $N_d \approx 1.5 n_d$ for the sake of robustness).*

Now, we want to compute the polynomial reconstructions based on the data of the associated stencil. To this end, we assume that vectors $\mathbb{U}_1 = (U_{1,k})_{k=I+1,\dots,I+K}$, $\mathbb{U}_2 = (U_{2,k})_{k=I+1,\dots,I+K}$, and $\mathbb{P} = (P_i)_{i=1,\dots,I}$ gather the approximations of the mean values of U_1 and U_2 over the diamond cells and P over the primal cells, *i.e.*

$$U_{1,k} \approx \frac{1}{|c_k|}\int_{c_k} U_1 \, \mathrm{d}x, \quad U_{2,k} \approx \frac{1}{|c_k|}\int_{c_k} U_2 \, \mathrm{d}x, \quad P_i \approx \frac{1}{|c_i|}\int_{c_i} P \, \mathrm{d}x.$$

3.2 Conservative reconstruction for primal cells

For each primal cell c_i, $i \in \mathcal{C}_\mathcal{M}$, the local polynomial approximation of the underlying solution P based on vector $\mathbb{P}$ of degree d is defined as

$$\boldsymbol{P}_i(x) = P_i + \sum_{1\leq|\alpha|\leq d} \mathcal{R}_i^\alpha \left[(x-m_i)^\alpha - M_i^\alpha\right],$$

where $\alpha = (\alpha_1, \alpha_2)$ with $|\alpha| = \alpha_1 + \alpha_2$ and the convention $x^\alpha = x_1^{\alpha_1} x_2^{\alpha_2}$, vector $\mathcal{R}_i = (\mathcal{R}_i^\alpha)_{1\leq|\alpha|\leq d}$ gathers the polynomial coefficients, and $M_i^\alpha = \frac{1}{|c_i|}\int_{c_i}(x-m_i)^\alpha \,\mathrm{d}x$ in order to guarantee the conservation property

$$\frac{1}{|c_i|}\int_{c_i} \boldsymbol{P}_i(x)\,\mathrm{d}x = P_i.$$

For a given stencil S_i, we consider the quadratic functional

$$E_i(\mathcal{R}_i) = \sum_{q\in S_i}\left[\frac{1}{|c_q|}\int_{c_q}\boldsymbol{P}_i(x)\,\mathrm{d}x - P_q\right]^2. \tag{6}$$

We denote by $\widehat{\mathcal{R}}_i$ the unique vector which minimizes the quadratic functional (6) and we set $\widehat{\boldsymbol{P}}_i(x)$ the polynomial which corresponds to the best approximation in the least squares sense.

3.3 Conservative reconstruction for diamond cells

For each diamond cell c_k, $k \in \mathcal{C}_\mathcal{D}$, the local polynomial approximation of the underlying functions U_1 and U_2 based on vectors $\mathbb{U}_1$ and $\mathbb{U}_2$ of degree d are defined as

$$\boldsymbol{U}_{\beta,k}(x) = U_{\beta,k} + \sum_{1\leq|\alpha|\leq d} \mathcal{R}_{\beta,k}^\alpha \left[(x-m_k)^\alpha - M_k^\alpha\right], \quad \beta = 1,2,$$

where vector $\mathcal{R}_{\beta,k} = (\mathcal{R}_{\beta,k}^\alpha)_{1\leq|\alpha|\leq d}$ gathers the polynomial coefficients and $M_k^\alpha = \frac{1}{|c_k|}\int_{c_k}(x-m_k)^\alpha \,\mathrm{d}x$ in order to guarantee the conservation property

$$\frac{1}{|c_k|}\int_{c_k} \boldsymbol{U}_{\beta,k}(x)\,\mathrm{d}x = U_{\beta,k}.$$

For a given stencil S_k, we consider the quadratic functional

$$E_{\beta,k}(\mathcal{R}_{\beta,k}) = \sum_{q\in S_k}\left[\frac{1}{|c_q|}\int_{c_q}\boldsymbol{U}_{\beta,k}(x)\,\mathrm{d}x - U_{\beta,q}\right]^2. \tag{7}$$

We denote by $\widehat{\mathcal{R}}_{\beta,k}$ the unique vector which minimizes the quadratic functional (7) and we set $\widehat{\boldsymbol{U}}_{\beta,k}(x)$ the polynomial which corresponds to the best approximation in the least squares sense.

3.4 Non-conservative reconstruction for inner diamond edges

For each inner diamond edge $e_{k\ell}$, $k \in \mathcal{C}_{\mathcal{D}}$, $\ell \in \nu(k)$, the local polynomial approximations of degree d of the underlying functions U_1 and U_2 are defined as

$$\boldsymbol{U}_{\beta,k\ell}(x) = \sum_{0\leq|\alpha|\leq d} \mathcal{R}^{\alpha}_{\beta,k\ell}(x - m_{k\ell})^{\alpha}, \quad \beta = 1, 2,$$

where vector $\mathcal{R}_{\beta,k\ell} = (\mathcal{R}^{\alpha}_{\beta,k\ell})_{0\leq|\alpha|\leq d}$ gathers the polynomial coefficients (notice that in this case $|\alpha|$ starts with 0 since no conservation property is required). For a given stencil $S_{k\ell}$ with $\#S_{k\ell}$ elements and vector $\omega_{\beta,k\ell} = (\omega_{\beta,k\ell,q})_{q=1,\ldots,\#S_{k\ell}}$ of the positive weights of the reconstruction, we consider the quadratic functional

$$E_{\beta,k\ell}(\mathcal{R}_{\beta,k\ell}) = \sum_{q\in S_{k\ell}} \omega_{\beta,k\ell,q} \left[\frac{1}{|c_q|}\int_{c_q} \boldsymbol{U}_{\beta,k\ell}(x)\,\mathrm{d}x - U_{\beta,q}\right]^2. \tag{8}$$

We denote by $\widetilde{\mathcal{R}}_{\beta,k\ell}$ the unique vector which minimizes the quadratic functional (8) and we set $\widetilde{\boldsymbol{U}}_{\beta,k\ell}(x)$ the polynomial which corresponds to the best approximation in the least squares sense.

3.5 Conservative reconstruction for diamond boundary edges

We treat the boundary diamond edges in a particular way in order to take into account the Dirichlet boundary conditions prescribed for the velocity. For each boundary diamond edge $e_{k\mathrm{D}}$, $k \in \mathcal{C}_{\mathcal{D}}$, the local polynomial approximations of degree d of the underlying functions U_1 and U_2 are defined as

$$\boldsymbol{U}_{\beta,k\mathrm{D}}(x) = U_{\beta,k\mathrm{D}} + \sum_{1\leq|\alpha|\leq d} \mathcal{R}^{\alpha}_{\beta,k\mathrm{D}}\left[(x - m_{k\mathrm{D}})^{\alpha} - M^{\alpha}_{k\mathrm{D}}\right], \quad \beta = 1, 2,$$

where vector $R_{\beta,k\mathrm{D}} = (R^{\alpha}_{\beta,k\mathrm{D}})_{1\leq|\alpha|\leq d}$ gathers the polynomial coefficients, $U_{\beta,k\mathrm{D}}$ is an approximation of the mean value $U_{\beta,\mathrm{D}}$ of order $2R$ over the diamond boundary edge $e_{k\mathrm{D}}$, and $M^{\alpha}_{k\mathrm{D}} = \frac{1}{|e_{k\mathrm{D}}|}\int_{e_{k\mathrm{D}}}(x - m_{k\mathrm{D}})^{\alpha}\,\mathrm{d}x$ in order to guarantee the conservation property

$$\frac{1}{|e_{k\mathrm{D}}|}\int_{e_{k\mathrm{D}}} \boldsymbol{U}_{\beta,k\mathrm{D}}(x)\,\mathrm{d}s = U_{\beta,k\mathrm{D}}.$$

For a given stencil $S_{k\mathrm{D}}$ with $\#S_{k\mathrm{D}}$ elements and vector $\omega_{\beta,k\mathrm{D}} = (\omega_{\beta,k\mathrm{D},q})_{q=1,\ldots,\#S_{k\mathrm{D}}}$ of the positive weights of the reconstruction, we consider the quadratic functional

$$E_{\beta,k\mathrm{D}}(\mathcal{R}_{\beta,k\mathrm{D}}) = \sum_{q\in S_{k\mathrm{D}}} \omega_{\beta,k\mathrm{D},q} \left[\frac{1}{|c_q|}\int_{c_q} \boldsymbol{U}_{\beta,k\mathrm{D}}(x)\,\mathrm{d}x - U_{\beta,q}\right]^2. \tag{9}$$

We denote by $\widehat{\mathcal{R}}_{\beta,k\mathrm{D}}$ the unique vector which minimizes the quadratic functional (9) and we set $\widehat{\boldsymbol{U}}_{\beta,k\mathrm{D}}(x)$ the polynomial which corresponds to the best approximation in the least squares sense.

Remark *The motivation for introducing the weights in the case of a non-conservative polynomial reconstruction and in the case of a conservative polynomial reconstruction for Dirichlet boundary edges, is presented in [5] as well as the importance to set larger values for the adjacent cells.*

3.6 High-order finite volume scheme

This subsection is dedicated to design high-order numerical flux approximations based on the polynomial reconstructions presented in the previous subsections to provide the global residual operator.

3.6.1 Numerical fluxes

For a given polynomial degree d and the associated stencils which guarantee the d-consistency property (see [5]), four numerical fluxes situations arise:

- for an inner diamond edge $e_{k\ell}$, the fluxes at the quadrature point $q_{k\ell,r}$ write

$$\mathcal{F}^U_{\beta,k\ell,r} = -\mu(q_{k\ell,r})\nabla\widetilde{\boldsymbol{U}}_{\beta,k\ell}(q_{k\ell,r})\cdot n_{k\ell} \quad \text{and} \quad \mathcal{F}^P_{\beta,k\ell,r} = \widehat{\boldsymbol{P}}_i(q_{k\ell,r})n_{\beta,k\ell}, \quad \beta = 1,2,$$

  with the correspondence $i = \Pi_{\mathcal{M}}(k,\ell)$;

- for a boundary diamond edge $e_{k\mathrm{D}}$, the fluxes at the quadrature point $q_{k\mathrm{D},r}$ write

$$\mathcal{F}^U_{\beta,k\mathrm{D},r} = -\mu(q_{k\mathrm{D},r})\nabla\widehat{\boldsymbol{U}}_{\beta,k\mathrm{D}}(q_{k\mathrm{D},r})\cdot n_{k\mathrm{D}} \quad \text{and} \quad \mathcal{F}^P_{\beta,k\mathrm{D},r} = \widehat{\boldsymbol{P}}_i(q_{k\mathrm{D},r})n_{\beta,k\mathrm{D}}, \quad \beta = 1,2,$$

  with the correspondence $i = \Pi_{\mathcal{M}}(k,\mathrm{D})$;

- for an inner primal edge e_{ij}, the flux at the quadrature point $q_{ij,r}$ writes

$$\mathcal{F}^{\nabla}_{ij,r} = \widehat{\boldsymbol{U}}_{1,k}(q_{ij,r})n_{1,ij} + \widehat{\boldsymbol{U}}_{2,k}(q_{ij,r})n_{2,ij},$$

  with the correspondence $k = \Pi_{\mathcal{D}}(i,j)$;

- for a boundary primal edge $e_{i\mathrm{D}}$, the flux at the quadrature point $q_{i\mathrm{D},r}$ writes

$$\mathcal{F}^{\nabla}_{i\mathrm{D},r} = \widehat{\boldsymbol{U}}_{1,k\mathrm{D}}(q_{i\mathrm{D},r})n_{1,i\mathrm{D}} + \widehat{\boldsymbol{U}}_{2,k\mathrm{D}}(q_{i\mathrm{D},r})n_{2,i\mathrm{D}},$$

  with the correspondence $k = \Pi_{\mathcal{D}}(i,\mathrm{D})$.

3.6.2 Residual operators

For any vector $\Phi = (\mathbb{U}_1, \mathbb{U}_2, \mathbb{P})$ in $\mathbb{R}^{2K+I}$, we define the residual operators for each diamond cell c_k, $k \in \mathcal{C}_D$, as

$$\mathcal{G}^{\beta}_k(\Phi) = \sum_{\ell\in\nu(k)} \frac{|e_{k\ell}|}{|c_k|}\left[\sum_{r=1}^{R}\zeta_r\left(\mathcal{F}^U_{\beta,k\ell,r} + \mathcal{F}^P_{\beta,k\ell,r}\right)\right] - f_{\beta,k}, \quad \beta = 1,2,$$

and for each primal cell c_i, $i \in \mathcal{C}_\mathcal{P}$, as

$$\mathcal{G}_i^\nabla(\Phi) = \sum_{j\in\nu(i)} \frac{|e_{ij}|}{|c_i|} \sum_{r=1}^{R} \zeta_r \mathcal{F}_{ij,r}^\nabla,$$

which correspond to the finite volume scheme (4-5) cast in residual form. Gathering all the components of the residuals in vectors $\mathcal{G}^\beta(\Phi) = \big(\mathcal{G}_k^\beta(\Phi)\big)_{k=I+1,\dots,I+K}$ and $\mathcal{G}^\nabla(\Phi) = \big(\mathcal{G}_i^\nabla(\Phi)\big)_{i=1,\dots,I}$, we introduce the global affine operator from $\mathbb{R}^{2K+I}$ into $\mathbb{R}^{2K+I}$, given by

$$\mathcal{H}(\Phi) = \big(\mathcal{G}^1(\Phi), \mathcal{G}^2(\Phi), \mathcal{G}^\nabla(\Phi)\big)^T,$$

such that vector $\Phi^\star = (\mathbb{U}_1^\star, \mathbb{U}_2^\star, \mathbb{P}^\star)^T \in \mathbb{R}^{2K+I}$, solution of the problem $\mathcal{H}(\Phi) = 0$, provides a constant piecewise approximation of U_1, U_2, and P.

4 DIRICHLET CONDITION ON CURVED BOUNDARY

When dealing with curved boundaries, the substitution of domain Ω with the polygonal domain deriving from the mesh dramatically reduces the method order due to a coarse approximation of the boundary by line segments. A specific treatment of the polynomial reconstruction associated to the edge on the boundary is required.

4.1 Second-order approach

Let e_{kD} be an edge of the dual mesh situated on the boundary Γ_D and set the mean value $\bar{U}_{\beta,kD} = \dfrac{1}{|e_{kD}|}\displaystyle\int_{e_{kD}} U_{\beta,D}(s)\, ds$ with $\beta = 1, 2$ the two components of the velocity. In [5] the following conservative polynomial function of degree d has been considered

$$\widehat{U}_{\beta,kD}(x;d) = U_{\beta,kD} + \sum_{1\le|\alpha|\le d} \mathfrak{R}_{\beta,kD}^{d,\alpha}\Big\{(x - m_{kD})^\alpha - M_{kD}^\alpha\Big\}, \tag{10}$$

taking $U_{\beta,kD} = \bar{U}_{\beta,kD}$, m_{kD} the midpoint of edge e_{kD} and $M_{kD}^\alpha = \dfrac{1}{|e_{kD}|}\displaystyle\int_{e_{kD}} (x - m_{kD})^\alpha\, ds$ such that the conservative property $\dfrac{1}{|e_{kD}|}\displaystyle\int_{e_{kD}} \widehat{U}_{\beta,kD}(x;d)\, ds = U_{\beta,kD}$ holds. To fix the coefficients, we introduce the functional

$$E_{\beta,kD}(\mathfrak{R}_{\beta,kD}^d; d) = \sum_{\ell\in S(e_{kD},d)} \omega_{\beta,kD,\ell}\Big[\frac{1}{|c_\ell|}\int_{c_\ell} \widehat{U}_{\beta,kD}(x;d)\, dx - U_{\beta,\ell}\Big]^2, \tag{11}$$

where $\omega_{\beta,kD,\ell}$ are positive weights and vector $\widehat{\mathfrak{R}}_{\beta,kD}^d$ stands for the unique vector minimizing the functional which provides the best approximation. Such an approach gives, at most, a second-order approximation since we substitute the mean value on a curved arc by the mean value on edge e_{kD} leading to a loose of accuracy. The keypoint is to evaluate the polynomial reconstruction with a better $U_{\beta,kD}$ choice, different to the candidate $\bar{U}_{\beta,kD}$, in order to provide better approximations of $\widehat{U}_{\beta,kD}(x;d)$ at the Gauss points $m_{kD,r}$, $r = 1, \cdots, R_2$.

4.2 High-order approximation

A local parametrization is introduced and a new quadrature formula is used to perform accurate numerical integration on the curved arc. Let e be a generic boundary edge, we denote by v_1 e v_2 the vertexes and denote $e = v_1v_2$ the segment with lenght $|v_1v_2|$ while $\widehat{v_1v_2}$ represents the boundary arc between v_1 and v_2 with length $|\widehat{v_1v_2}|$. We introduce the edge parametrization $q(t) = (1-t)v_1 + tv_2$, $t \in [0,1]$ which satisfies $|q'(t)| = |v_1v_2|$ while $p(t)$ is a parametrization of the arc such that

$$p(0) = v_1,\ p(1) = v_2,\ |p'(t)| = |\widehat{v_1v_2}| \text{ is constant.}$$

Let us denote by q_1, ..., q_{R_2} the Gauss points on edge e associated to parameters t_1, ..., t_{R_2}, then $p_1 = p(t_1)$, ..., $p_{R_2} = p(t_{R_2})$ are the corresponding Gauss points on the boundary arc. Indeed, using the quadrature rule for the numerical integration over the arc, one has

$$\int_{\widehat{v_1v_2}} U_{\beta,D}(p)dp = \int_0^1 U_{\beta,D}(p(t))|p'(t)|dt \approx \sum_{r=1}^{R_2} \xi_r U_{\beta,D}(p_r)|p'(t_r)| = |\widehat{v_1v_2}| \sum_{r=1}^{R_2} \xi_r U_{\beta,D}(p_r).$$

Notice that the following property then holds for $r = 1, \cdots, R_2$

$$\frac{|\widehat{v_1p_r}|}{|v_1q_r|} = \frac{|\widehat{v_2p_r}|}{|v_2q_r|} = \frac{|\widehat{v_1v_2}|}{|v_1v_2|}.$$

Let us now consider $\widehat{e}_{kD}$ the boundary arc associated to the edge e_{kD} and assume that the mean value approximations U_i, are given on the stencil. We consider the following linear operator

$$U_{\beta,kD} \to \widehat{U}_{\beta,kD}(x; d, U_{\beta,kD}) \in \mathbb{P}_d$$

where $U_{\beta,kD}$ represents an approximation of the mean value on e_{kD} **and not** on $\widehat{e}_{kD}$ and is seen as a free parameter. The main difficulty is that the Dirichlet condition is defined on $\widehat{e}_{kD}$ **and not** on e_{kD}. To overcome the problem we introduce the functional

$$H(U_{\beta,kD}) = \sum_{r=1}^{R_2} \left(\widehat{U}_{\beta,kD}(p_{kD,r}; d, U_{\beta,kB}) - U_{\beta,D}(p_{kD,r})\right)^2$$

which corresponds to the error at the boundary arc Gauss points between the polynomial approximation and the real Dirichlet condition. Since we are dealing with a quadratic functional, existence and uniqueness of the minimum $U^\star_{\beta,kD}$ is guaranteed and $\widehat{U}_{\beta,kD}$ will be the polynomial reconstruction where we take $U_{\beta,kD} = U^\star_{\beta,kD}$.
To compute $U^\star_{\beta,kD}$ in practice, we propose the following simple algorithm. We consider the sequence $(U^n_{\beta,kD})^n$ initialized with $U^0_{\beta,kD} = \bar{U}_{\beta,kD}$ and given by the following:

1. with $U^n_{\beta,kB}$ in hand, compute the associated polynomial function $\widehat{U}_{\beta,kD}(x; d, U^n_{\beta,kB})$,

2. evaluate the errors $\delta_r^n = U_{\beta,D}(p_{kD,r}) - \widehat{U}_{\beta,kD}^n(p_{kD,r}; d, U_{\beta,kB}^n)$,

3. update the mean value on e_{kD} with $U_{\beta,kD}^{n+1} = U_{\beta,kD}^n + \sum_{r=1}^{R_2} \xi_r \delta_r^n$,

4. stop if $|U_{\beta,kD}^{n+1} - U_{\beta,kD}^n| < \epsilon_B \bar{U}_{\beta,nD}$ where the tolerance ϵ_B has been prescribed and set $U_{\beta,kD}^\star = U_{\beta,kD}^{n+1}$, else goto step (1).

Numerical experiments shows that we quickly converge with two or three steps using $\epsilon_B = 10^{-12}$. Furthermore, when $\bar{U}_{\beta,kD} = 0$, we use the absolute error criterion $|U_{\beta,kD}^{n+1} - U_{\beta,kD}^n| < \epsilon_B$ in place of the relative error criterion. Remark *Notice that the method only requires the arc length $|\widehat{e}_{kD}|$ and the Gauss point $p_{kD,r}$ on the boundary arc. No geometrical tranformation is performed which provides a very simple method, easy to implement.*

5 NUMERICAL RESULTS

To perform the numerical tests, we consider a fluid with viscosity $\mu = 1$ flowing in a circlar domain $\Omega = \{x : \tau^2 < 1\}$ where $\tau^2 = x_1^2 + x_2^2$. In order to check the implementation of the method and assess the convergence rates, we manufacture an analytical solution for the given problem setting

$$U_1(x) = -ay\exp(\tau^2)(1-\tau), \quad U_2(x) = ax\exp(\tau^2)(1-\tau), \quad P(x) = \cos(\pi\tau^2),$$

where $a = 1/\left((1/(2\sqrt{2}))\exp(1/2)\right)$ in order to normalize the velocity. Then, the source terms are computed such that equations (1) and (2) hold. The homogeneous Dirichlet boundary condition $U_{\mathrm{D}}(x) = (0,0)$ prescribed on $\partial\Omega$, derives from de exact solution. Vectors $\mathbb{U}_\beta^\star = (U_{\beta,k}^\star)_{k\in\mathcal{C}_\mathcal{D}}$, $\beta = 1,2$, and $\mathbb{P}^\star = (P_i^\star)_{i\in\mathcal{C}_\mathcal{M}}$ gather the approximate mean values while vectors $\overline{\mathbb{U}}_\beta = (\overline{U}_{\beta,k})_{k\in\mathcal{C}_\mathcal{D}}$, $\beta = 1,2$, and $\overline{\mathbb{P}} = (\overline{P}_i)_{i\in\mathcal{C}_\mathcal{M}}$ gather the exact mean values of the solution given by

$$\overline{U}_{\beta,k} = \frac{1}{|c_k|}\int_{c_k} U_\beta \,\mathrm{d}x, \beta = 1,2, \quad \text{and} \quad \overline{P}_i = \frac{1}{|c_i|}\int_{c_i} P \,\mathrm{d}x.$$

The L^1-norm errors are given by

$$E_1^\beta(\mathcal{D}) = \frac{\sum_{k\in\mathcal{C}_\mathcal{D}} |U_{\beta,k}^\star - \overline{U}_{\beta,k}||c_k|}{\sum_{k\in\mathcal{C}_\mathcal{D}} |c_k|}, \beta = 1,2, \quad \text{and} \quad E_1^P(\mathcal{M}) = \frac{\sum_{i\in\mathcal{C}_\mathcal{M}} |P_i^\star - \overline{P}^\star - \overline{P}_i - \overline{P}||c_i|}{\sum_{i\in\mathcal{C}_\mathcal{M}} |c_i|},$$

and the L^∞-norm errors are given by

$$E_\infty^\beta(\mathcal{D}) = \max_{k\in\mathcal{C}_\mathcal{D}} |U_{\beta,k}^\star - \overline{U}_{\beta,k}|, \beta = 1,2, \quad \text{and} \quad E_\infty^P(\mathcal{M}) = \max_{i\in\mathcal{C}_\mathcal{M}} |P_i^\star - \overline{P}^\star - \overline{P}_i - \overline{P}|.$$

where $\overline{P^\star}$ is the mean value of the values gather in vector $\mathbb{P}^\star$ and $\overline{P}$ is the mean value of the values gather in vector $\overline{\mathbb{P}}$, given by

$$\overline{P^\star} = \frac{\sum\limits_{i\in\mathcal{C}_\mathcal{M}} P_i^\star |c_i|}{\sum\limits_{i\in\mathcal{C}_\mathcal{M}} |c_i|}, \qquad \overline{P} = \frac{\sum\limits_{i\in\mathcal{C}_\mathcal{M}} \overline{P}_i |c_i|}{\sum\limits_{i\in\mathcal{C}_\mathcal{M}} |c_i|},$$

respectively, to guarantee a solution with null mean value pressure.
We evaluate the convergence rate of the L^1-norm (and L^∞-norm error) between two different and successive finer primal meshes $\mathcal{M}_1$ and $\mathcal{M}_2$, with I_1 and I_2 cells, respectively, as

$$O_1^P(\mathcal{M}_1,\mathcal{M}_2) = 2\frac{|\log(E_1^P(\mathcal{M}_1)/E_1^P(\mathcal{M}_2))|}{|\log(I_1/I_2)|}.$$

In the same way, we define the convergence order between two different and successive finer diamond meshes $\mathcal{D}_1$ and $\mathcal{D}_2$ with K_1 and K_2 cells, respectively, as

$$O_1^\beta(\mathcal{D}_1,\mathcal{D}_2) = 2\frac{|\log(E_1^\beta(\mathcal{D}_1)/E_1^\beta(\mathcal{D}_2))|}{|\log(K_1/K_2)|}.$$

In all the simulations we have carried out, the weights in functional (8) are set $\omega_{\beta,k\ell,q} = 3$, $k \in \mathcal{C}_\mathcal{D}$, $\ell \in \nu(k)$, $q \in S_{k\ell}$, $\beta = 1,2$, if $e_{k\ell}$ is an edge of c_q and $\omega_{\beta,k\ell,q} = 1$, otherwise, following [5].

The second-order case As a first test, we consider the classical polynomial reconstruction on the boundary given in Section 4.1 using the straithforward method computing the Dirichlet condition on the edge. We carry out simulations with successive finer regular triangular Delaunay meshes and the associated diamond meshes and report in Tables 1, 2, 3 the L^1- and L^∞-norm errors and the convergence rates using the $\mathbb{P}_1$, $\mathbb{P}_3$, and $\mathbb{P}_5$ polynomial reconstructions, respectively. Notice that the number of unknowns (the same as degrees of freedom) is $DOF = K$ for U_1 and U_2 and $DOF = I$ for P. The notation E_1 is a generalization which stands for E_1^β or E_1^P depending on the variable we are dealing with (U_β or P, respectively). The same convention is valid for E_∞, O_1, and O_∞.
The $\mathbb{P}_1$ polynomial reconstruction provides a second-order approximation for the velocity and a first-order approximation for the pressure, as expected. The schemes based on the $\mathbb{P}_3$ and $\mathbb{P}_5$ polynomial reconstructions, also provides second-order convergence rates for the velocity since the reconstruction on dual boundary edges is of second-order. Inspite of this negative results, the scheme achieves a third-order covergence for the pressure with $\mathbb{P}_3$ and $\mathbb{P}_5$ polynomial reconstructions. Such situation arises since the null-velocity boundary condition guarantees that the divergence on $e_{k\mathrm{D}}$, $k \in \mathcal{C}_\mathcal{M}$ is very close to zero, the exact flux.

Table 1: Errors and convergence rates with $\mathbb{P}_1$ polynomial reconstructions where the polynomials on boundary edges are computed according to Section 4.1.

	DOF	E_1	O_1	E_2	O_2	E_∞	O_∞
U_1	1337	1.66E−02	—	2.03E−02	—	4.77E−02	—
	2486	8.83E−03	2.03	1.06E−02	2.08	2.97E−02	1.53
	9835	2.30E−03	1.96	2.80E−03	1.94	8.17E−03	1.88
	21337	1.02E−03	2.10	1.24E−03	2.10	3.70E−03	2.05
U_2	1337	1.67E−02	—	2.03E−02	—	4.73E−02	—
	2486	8.79E−03	2.07	1.07E−02	2.08	2.97E−02	1.50
	9835	2.30E−03	1.95	2.80E−03	1.95	8.44E−03	1.83
	21337	1.02E−03	2.11	1.24E−03	2.10	3.68E−03	2.14
P	870	7.89E−02	—	1.42E−01	—	6.21E−01	—
	1628	5.42E−02	1.20	9.83E−02	1.17	4.35E−01	1.13
	6498	2.21E−02	1.30	4.03E−02	1.29	2.48E−01	0.81
	14138	1.47E−02	1.06	2.58E−02	1.14	1.55E−01	1.20

Table 2: Errors and convergence rates with $\mathbb{P}_1$ polynomial reconstructions where the polynomials on boundary edges are computed according to Section 4.1.

	DOF	E_1	O_1	E_2	O_2	E_∞	O_∞
U_1	1337	3.07E−03	—	3.63E−03	—	7.41E−03	—
	2486	1.65E−03	2.00	1.95E−03	2.01	3.90E−03	2.07
	9835	4.18E−04	2.00	4.93E−04	2.00	9.85E−04	2.00
	21337	1.92E−04	2.00	2.27E−04	2.01	4.53E−04	2.01
U_2	1337	3.08E−03	—	3.63E−03	—	7.41E−03	—
	2486	1.65E−03	2.01	1.95E−03	2.01	3.90E−03	2.07
	9835	4.19E−04	1.99	4.93E−04	2.00	9.87E−04	2.00
	21337	1.92E−04	2.01	2.27E−04	2.01	4.53E−04	2.01
P	870	1.41E−03	—	2.23E−03	—	9.77E−03	—
	1628	5.08E−04	3.26	8.19E−04	3.20	3.74E−03	3.07
	6498	6.13E−05	3.06	1.01E−04	3.03	5.50E−04	2.77
	14138	1.87E−05	3.05	3.11E−05	3.03	2.29E−04	2.25

The high-order case We now consider the high-oder polynomial polynomial reconstruction on the boundary using the correction given in Section 4.2. We carry out simulations with successive finer regular meshes.

We report in Tables 4, 5, and 6 the L^1- and L^∞-norm errors and the convergence rates using the $\mathbb{P}_1$, $\mathbb{P}_3$, and $\mathbb{P}_5$ polynomial reconstructions, respectively.

As in the previous case, the $\mathbb{P}_1$ polynomial reconstruction provides a second-order approximation for the velocity and a first-order approximation for the pressure. The scheme based on the $\mathbb{P}_3$ reconstruction achieves an effective fourth-order approximation for the

Table 3: Errors and convergence rates with $\mathbb{P}_5$ polynomial reconstructions where the polynomials on boundary edges are computed according to Section 4.1.

	DOF	E_1	O_1	E_2	O_2	E_∞	O_∞
U_1	1337	3.16E−03	—	3.73E−03	—	7.40E−03	—
	2486	1.68E−03	2.04	1.98E−03	2.05	3.93E−03	2.04
	9835	4.20E−04	2.02	4.95E−04	2.02	9.86E−04	2.01
	21337	1.93E−04	2.01	2.27E−04	2.01	4.53E−04	2.01
U_2	1337	3.16E−03	—	3.73E−03	—	7.40E−03	—
	2486	1.68E−03	2.04	1.98E−03	2.05	3.93E−03	2.04
	9835	4.20E−04	2.02	4.95E−04	2.02	9.86E−04	2.01
	21337	1.93E−04	2.01	2.27E−04	2.01	4.53E−04	2.01
P	870	3.23E−05	—	5.09E−05	—	2.54E−04	—
	1628	7.28E−06	4.76	1.23E−05	4.53	5.57E−05	4.84
	6498	3.15E−07	4.54	1.04E−06	3.57	2.56E−05	1.12
	14138	7.06E−08	3.85	3.33E−07	2.93	9.07E−06	2.67

Table 4: Errors and convergence rates with $\mathbb{P}_1$ polynomial reconstructions where the polynomials on boundary edges are computed according to Section 4.2.

	DOF	E_1	O_1	E_2	O_2	E_∞	O_∞
U_1	1337	2.01E−02	—	2.44E−02	—	5.50E−02	—
	2486	1.07E−02	2.03	1.28E−02	2.07	3.40E−02	1.55
	9835	2.77E−03	1.96	3.35E−03	1.95	9.26E−03	1.89
	21337	1.24E−03	2.08	1.49E−03	2.09	4.19E−03	2.05
U_2	1337	2.03E−02	—	2.44E−02	—	5.52E−02	—
	2486	1.07E−02	2.08	1.28E−02	2.07	3.40E−02	1.57
	9835	2.77E−03	1.97	3.35E−03	1.95	9.53E−03	1.85
	21337	1.23E−03	2.09	1.49E−03	2.09	4.17E−03	2.13
P	870	7.86E−02	—	1.41E−01	—	6.20E−01	—
	1628	5.42E−02	1.19	9.82E−02	1.15	4.36E−01	1.13
	6498	2.21E−02	1.30	4.03E−02	1.29	2.47E−01	0.82
	14138	1.47E−02	1.06	2.58E−02	1.15	1.55E−01	1.20

velocity and a third-order (slightly better) approximation for the pressure. The scheme based on the $\mathbb{P}_5$ reconstruction achieves a sixth- and fifth-order approximations for the velocity and the pressure, respectively, which demonstrates the effectiveness of the correction. Finally, we also mention that no oscillations or numerical locking are reported in all the experiences.

Table 5: Errors and convergence rates with $\mathbb{P}_3$ polynomial reconstructions where the polynomials on boundary edges are computed according to Section 4.2.

	DOF	E_1	O_1	E_2	O_2	E_∞	O_∞
U_1	1337	1.00E−04	—	1.25E−04	—	4.10E−04	—
	2486	2.69E−05	4.23	3.45E−05	4.15	1.13E−04	4.16
	9835	1.89E−06	3.86	2.35E−06	3.91	9.93E−06	3.54
	21337	2.90E−07	4.84	3.99E−07	4.58	2.53E−06	3.53
U_2	1337	9.18E−05	—	1.20E−04	—	4.36E−04	—
	2486	2.70E−05	3.94	3.36E−05	4.10	1.14E−04	4.34
	9835	1.81E−06	3.93	2.33E−06	3.88	1.26E−05	3.20
	21337	2.90E−07	4.73	3.97E−07	4.57	2.67E−06	4.00
P	870	1.40E−03	—	2.21E−03	—	9.54E−03	—
	1628	5.06E−04	3.25	8.15E−04	3.18	3.69E−03	3.03
	6498	6.12E−05	3.05	1.00E−04	3.03	5.49E−04	2.75
	14138	1.87E−05	3.05	3.10E−05	3.01	2.29E−04	2.25

Table 6: Errors and convergence rates with $\mathbb{P}_5$ polynomial reconstructions where the polynomials on boundary edges are computed according to Section 4.2.

	DOF	E_1	O_1	E_2	O_2	E_∞	O_∞
U_1	1337	4.18E−06	—	5.13E−06	—	1.38E−05	—
	2486	6.17E−07	6.17	7.87E−07	6.04	2.52E−06	5.48
	9835	1.30E−08	5.61	1.63E−08	5.64	4.91E−08	5.73
	21337	1.20E−09	6.15	1.51E−09	6.14	4.91E−09	5.94
U_2	1337	4.24E−06	—	5.15E−06	—	1.29E−05	—
	2486	6.14E−07	6.23	7.90E−07	6.05	2.50E−06	5.30
	9835	1.30E−08	5.61	1.63E−08	5.64	5.22E−08	5.63
	21337	1.20E−09	6.16	1.51E−09	6.14	5.87E−09	5.64
P	870	3.15E−05	—	4.81E−05	—	2.09E−04	—
	1628	6.98E−06	4.81	1.14E−05	4.60	4.73E−05	4.74
	6498	2.01E−07	5.13	3.35E−07	5.10	1.99E−06	4.58
	14138	2.93E−08	4.96	4.96E−08	4.91	3.01E−07	4.86

6 CONCLUSION

We have presented a powerful method to derived an effective sixth-order of approximation for the Stokes equations involving curved boundary. We highlight that straightforward approximation will provide at most a second-order approximation leading to a huge degradation of the accuracy. The method is very simple to implement and only requires the Gauss points on the curved boundary. It can be seen as a blackbox to improve the accuracy since the structure of the polynomial reconstruction (we mean the matrix which compute the polynomial coefficients) is independant of the position of the Gauss points.

Consequently, the approximation of curved boundaries is just a plug-in function which enable to use the polygonal domain and add a small correction provinding the optimal order.

ACKNOWLEDGEMENTS

This research was financed by FEDER Funds through Programa Operational Fatores de Competitividade — COMPETE and by Portuguese Funds FCT — Fundação para a Ciência e a Tecnologia, within the Projects PEst-C/MAT/UI0013/2014, PTDC/MAT/121185/2010 and FCT-ANR/MAT-NAN/0122/2012.

References

REFERENCES

[1] Barth, T.J., Frederickson, P.O., "Higher order solution of the Euler equations on unstructured grids using quadratic reconstruction", *AIAA Paper* Vol. **90-0013**, 1990.

[2] Barth, T.J., "Recent developments in high order k-exact reconstruction on unstructured meshes", *AIAA Paper* Vol. **93-0668**, 1993.

[3] Boersma, B.J., "A 6th order staggered compact finite difference method for the incompressible Navier-Stokes and scalar transport equations", *J. Comput. Phys.* Vol. **230**, pp. 4940-4954, 2011.

[4] Boularas, A., Clain, S., Baudoin, F., "A sixth-order finite volume method for diffusion problem with curved boundaries", HAL preprint, https://hal.archives-ouvertes.fr/hal-01052517.

[5] Clain, S., Machado, G.J., Nóbrega, J.M., Pereira, R.M.S., "A sixth-order finite volume method for the convection-diffusion problem with discontinuous coefficients", *Comput. Meth. in App. Mech. and Eng.* Vol. **267**, pp. 43-64, 2013.

[6] Ferrer, E., Willden, R.H.J., "A high order discontinuous Galerkin finite element solver for the incompressible Navier-Stokes equations", *Comput. & Fluids* Vol. **46**, pp. 224-230, 2011.

[7] Ferziger, J.H., Perić,, "Computational methods for fluids dynamics", Springer-Verlag, Berlin, 1996.

[8] Frochte, J., Heinrichs, W., "A splitting technique of higher order for the Navier-Stokes equations", *J. Comput. and App. Math.* Vol. **228**, pp. 373-390, 2009.

[9] Griffith, B.E., "An accurate and efficient method for the incompressible Navier-Stokes equations using the projection method as preconditioner", *J. Comput. Phys.* Vol. **228**, pp. 7565-7595, 2009.

[10] Guermont, J.L., Minev, P., Shen, J., "An overview of the projection methods for incompressible flows", *Comput. Meth.Appl. Engrg.* Vol. **195**, pp. 6011-6045, 2006.

[11] R.-S. Hirsh, Higher order accurate difference solutions of fluid mechanics problems by a compact differencing technique, J. Comput. Phys. Vol. **19**, pp. 90-109, 1975.

[12] Kampanis, N.A., Ekaterinaris, J.A., "A staggerid grid, high-order accurate method for the incompressible Navier-Stokes Equations", *J. Comput. Phys.* Vol. **215**, pp. 589-613, 2006.

[13] Montlaur,A. , Fernandez-Mendez, S., Huerta, A., "Discontinuous Galerkin methods forthe Stokes equations using divergence-free approximations", *Inter. J. Numer. Meth. Fluids* **57**, pp. 1071-1092, 2008.

[14] Nigro, A., De Bartolo, C., Bassi, F., Ghidoni, A., "Up to sixth-order accurate A-stable implicit schemes applied to the discontinuous Galerkin discretized Navier-Stokes equations", *J. Comput. Phys.* Vol. **274**, pp. 136-162, 2014.

[15] Ollivier-Gooch,C. , Van Altena,M. , "A high-order-accurate unstructured mesh finite-volume scheme for the advection-diffusion equation", *J. Comput. Phys. Arch.* Vol. **181(2)**, pp. 729-752, 2002.

[16] Patankar,S.V. , "Numerical heat transfer and fluid flow", Hemisphere, New-York, 1980.

[17] Rhie, C. M., Chow, W.L., "A numerical study of the turbulent flow past an isolated airfoil with trailing edge separation", *AIAA J.* Vol. **21**, pp. 1525-1532, 1983.

[18] Sadd,Y., Schultz, M.H., "GMRES: a general minimal residual algorithm for solving nonsymmetric linear systems", *SIAM J. Sci. Stat. Comput.* Vol. **7(3)**, pp. 856-869,1986.

[19] Saad, Y., "Iterative methods for spares linear systems", Society for Industrial and Applied Mathematics, 2003.

[20] Shang, X., Zhao, V., Bayyuk, V., "Generalized formulations for the Rhie-Chow interpolation", *J. Comput. Phys.* Vol. **258**, pp. 880-914, 2014. Butterworth-Heinemann, Waltham, 2014.